SHEAR FRACTURE MECHANISM IN A RECYCLED ALUMINIUM ALLOY

D. M. LI[1] @ and A. BAKKER[2]

[1] *School of Materials Science & Engineering, Harbin Institute of Technology, Harbin 150001, China*

[2] *Department of Materials Science, Delft University of Technology, 2628 AL Delft, The Netherlands.*

ABSTRACT

The shear fracture mechanism was investigated using both smooth and circumferentially-notched bars under uniaxial tension in a temperature range of 193K - 423K and a strain rate range of $10^{-5} \sim 1\ s^{-1}$, for an aluminium scrap alloy under as-extruded and precipitation-hardened conditions post a rapid-solidification. An analytical procedure was performed to make corrections on the hydrostatic stresses in the necked region of a smooth specimen. The interfacial delamination is associated with both the complete shear fracture in plain tension and the local shearing in notch tension. A constraint-releasing mechanism is proposed to account for the interaction between metallurgical and mechanical variants.

KEYWORDS

Shear fracture, delamination, constraint effect, temperature and strain rate dependence, recycled aluminum alloy

INTRODUCTION

For commercial alloys under nominally non-plane-stress conditions, there is no unified theory to account for the mechanism of shear fracture, due to the complexity of the mechanical and metallurgical influencers involved. However, some significant factors promoting shear fracture are approached, assuming shear fracture to be a process or a consequence of localised or unstable flow (Backofen, 1964; Chung, *et al*, 1977; King, *et al*, 1981; Chen and Li, 1987). Backofen (1964) proposed a critical strain above which flow instability initiates, predicting that the susceptibility of a material to the unstable flow increases with decreasing strain-hardening rate or strain rate sensitivity or stiffness of test device but with increasing strain rate or the material's specific heat. Among these influencers the specific heat of the material reflects a

@ Present address: Department of Materials Science & Engineering, Pohang University of Science and Technology, Pohang 790-784, Korea

thermal softening effect which affects the flow localisation by inducing an adiabatic deformation, with the softening effect enhanced at low temperatures or high strain rates (Rohd, 1973). The other influencers reflect mechanical softening effects. From the negative free energy requirement, Chung *et al* (1977) proposed a criterion for the flow localisation, suggesting that a negative strain rate sensitivity of flow stress (strain rate softening) and/or a negative strain-hardening rate (strain softening) is required for the occurrence of the flow localisation. It should be noted that these models do not provide adequate information specific to shear fracture, since unstable deformation or plastic instability actually includes processes other than shear fracture, such as the necking process and the serrated flow. More recently Chen and Li (1987) extended the criterion for shear localisation in single crystals (Asaro, 1979; Peirce, *et al,* 1982), namely, that the ratio of the slip plane strain-hardening rate to the current tensile stress reaches a critical value, to predict the macroscopic shear localisation in polycrystalline commercial Al alloys. However, the validity for this extension is not verified in their study except that the value of the critical ratio at fracture is evaluated according to the fracture mode. It appears that more systematic investigations need to be carried out to understand the mechanism of shear fracture under a definite condition. The present study is conducted to investigate the mechanism of the shear fracture in an aluminum scrap alloy upon a rapid solidification.

EXPERIMENTAL

The material used was an aluminium scrap alloy having chemical composition of , in weight percent, 7.0 Si, 2.7 Cu, 1.5 Zn, 1.1 Fe, 0.3 Mn, 0.3 Mg, 0.1 Cr, 0.1 Ni, 0.04 Ti, and balance Al. The alloy was received in the form of recycled pilot units extruded in an industrial scrap processing plant in the Netherlands. Before extrusion the alloy underwent a rapid solidification processing called melt spinning, *i.e.* the melt was directed onto a copper wheel spinning at a high speed to provide a cooling rate of about 10^6 K/s, yielding thin ribbons. Then these ribbons were chopped into flakes and compacted into preforms for the convenience of further forming. The extrusion was performed at a temperature around 723 K with an extrusion ratio of 33:1. Another patch of samples were heat-treated upon extrusion. They were heated to 723 K and held for 15 minutes, quenched in water, and aged at 423 K for 24 hours, reaching a peak hardness. Both smooth round bar and circumferentially-notched round bar specimens were machined for tensile tests, with their longitudinal (tensile) axes in the extrusion direction. The smooth specimen had a diameter of 8 *mm* and a gauge length of 40 *mm*. The notched specimen had a gross diameter of 10 *mm* for a gauge length of 100 *mm*, at the centre of which a 60° V-notch was circumferentially cut with a depth of 2 *mm* and a root radius of 0.25 *mm*. All tensile tests were performed in an Instron 4505 testing machine equipped with a data-processing computer system. For the smooth specimens, the tests were conducted at different temperatures ranging from 193 K to 423 K and an apparent strain rate range of 10^{-5} - 1 s^{-1}. The notched specimens were only pulled at room temperature and a cross-head speed of 2 *mm/min*. The contour of the necked volume was measured for each smooth specimen using a microscopic ruler. Observations under both the optical microscope and the scanning electron microscope (SEM) were made to examine metallurgical and fractographic details.

RESULTS AND DISCUSSION

Temperature and Strain Rate Dependence of Plain Tensile Behavior

The as-extruded (AE) alloy exhibits a positive strain rate sensitivity of flow stress (an increase in stress - strain envelope with increasing strain rate) at temperatures higher than 353K or lower than 233K, but exhibits a negative sensitivity (a decrease in stress - strain envelope with increasing strain rate) in the temperature range of 293 - 313K, regardless of strain rate. At temperatures between 333K and 353K, the sensitivity is positive in the low strain rate range but turns negative in the high strain rate range, whereas it is negative only at low strain rates at 233K. Therefore the negative sensitivity occurs only for a specific temperature-strain rate combination. The strain hardening exponent n, as defined in the Holloman equation for the true stress (σ) *vs* true strain (ε), $\sigma = K\varepsilon^n$, accounts for the trend of flow stress: an increase in n corresponds to an increase in flow stress, and *vice versa*. The values of n vary with temperature and strain rate, ranging between 0.15 and 0.23. At a definite strain rate, the general trend of the decrease in tensile flow stress with increasing temperature is retarded, or held, in the intermediate temperature range (293-313 K). Similarly, at a definite temperature, the general trend of the decrease in reduction of area (*RA*) with increasing strain rate also gets retarded in the same intermediate temperature range. On the other hand, the heat-treated (HT) alloy shows a monotonic dependence of the tensile behavior on temperature and strain rate. It gives a positive sensitivity independent of temperature or strain rate rang. The strain hardening exponent n is smaller than that of the AE alloy, being 0.10 - 0.14 for varied temperatures and strain rates. For a definite strain rate, the flow stress decreases with increasing temperature. *RA* decreases with increasing strain rate for a given temperature and increases with increasing temperature for a given strain rate. Detailed data are available elsewhere (Li and Bakker, 1995).

Fractographic Observations

In plain tension, all the HT specimens are broken in a normal fracture mode with a "cup-cone" fracture surface regardless of temperature and strain rate. For the AE group, when temperature is higher than 353K or lower than 233K, the fracture is also by the same normal mode. A typical shear fracture is only found in the temperature range between 233K and 353K for specific strain rates detailed in the forthcoming section. The micro-mechanism of the shear fracture is micro-void coalescence evidenced by the dimple pattern on the fracture surface, with the difference from the normal fracture in that the stretched dimples appears, in place of the equiaxed one. On a pure shear fracture surface, some secondary cracks are found in the central region (Fig. 1-a). With tilting the surface at an angle of ~ 45°, the profile of the secondary crack reveals an evidence characteristic of interfacial debonding or delamination (Fig. 1-b). By sectioning the necked area of a specimen unloaded just before fracture, micro-cracks are frequently found in the longitudinal orientation (Fig. 1-c). These features are characteristic of the AE alloy: they are not evidenced in the HT alloy. The notch tensile test is aimed to confirm the susceptibility of the alloy to interfacial delamination since this test is advantageous over the plain tensile test in that the constraint is intensified by a notch. The AE specimen has a macroscopically flat contour perpendicular to the tensile axis. However, the appearance of delamination is clearly evidenced on the fracture surface, especially as is shown on the profile of longitudinally-sectioned specimen (Fig. 1-d). It is indicated that the delaminated interfaces have an appearance much like that found in the smooth tensile specimens (comparing Fig. 1-e with 1-b). The local slant (shear) fracture occurs between the delaminations, as is shown in Fig. 1-d. These slant surfaces are

characterised by stretched dimples and ridges (Fig. 1-f), suggesting a shearing process. For the HT alloy, the extent of delamination is greatly decreased regarding both the density and the magnitude.

Stress Analysis for the Necked Region

Considering the interfacial delamination found in the necked region of the plain tensile specimen, it appears necessary to evaluate the stress state in that region. For this purpose a correction on the hydrostatic stress has to be made. Bridgeman (1952) originated this correction and established both the constitutive relations and experimental data base obtained from a series of alloys. The present analysis is based on Bridgeman's correction model since there are sufficient direct experimental data obtained under different strain-hardening values. Data of the relative neck curvature a/R (a = specimen radius at neck, R = radius of neck curvature) are required to calculate hydrostatic stresses. Experimental values of a/R are obtained as a function of the true plastic strain at neck (true fracture strain for the present case). These data fall on the upper bound of the previous experimental data of a/R collected on a series of alloys including steels, bronzes and brasses (Bridgeman, 1952). Note that a/R reflects geometrically the degree of strain concentration around necked region, here the high a/R value for a definite strain implies that the flow localisation is a protruding issue for the alloy used. Having a/R data, the ratio of flow stress (σ_f) to the mean axial stress (σ_{ax}), called the correction factor (CF), can be calculated according to (Bridgeman, 1952)

$$CF = \sigma_f / \sigma_{ax} = 1 / (1 + 2R / a) / ln[1 + a / (2R)] \qquad (1)$$

Using the data of the mean axial stress σ_{ax} [$= P/(\pi a^2)$ where P is tensile load] at fracture, the corrected fracture stress σ_F can be obtained by calculating σ_f at the point of fracture with Eq. 1. Fig. 2-a gives a map of σ_F values for all specimens fractured by a pure shear mode at different temperatures and strain rates (the pure shear fracture family). It is found that these σ_F values fall into a narrow range of 351 - 372 MPa. Then the two transverse stress components, namely, the radial stress σ_{rr} and the circumferential stress $\sigma_{\theta\theta}$ can be estimated using the relation

$$\sigma_{rr} = \sigma_{\theta\theta} = \sigma_f ln[1 + a / (2R) - r^2 / (2aR)] \qquad (2)$$

where r is the radial co-ordinate originating at the central point of the specimen cross section. The values of σ_{rr} at fracture for $r = 0$ are given in Fig. 2-b for all specimens of the pure shear fracture family. Similarly, the σ_{rr} ($r = 0$) values also fall within a narrow range of 52 - 64 MPa. The σ_F and σ_{rr} ($r = 0$) values for the smooth specimens other than the pure shear fracture family are generally lower than the range indicated above.

Discussion on Fracture Mechanism

In the present study, shear fracture occurs in the AE alloy but not in the HT alloy while the strain hardening exponent is higher in the former than in the latter. Even for the AE alloy shear fracture is evident in a temperature range where a peak of the strain hardening exponent appears. This is in contradiction to the conventional argument that a low strain hardening rate should

facilitate shear fracture (Backofen, 1964). The negative strain rate sensitivity is previously assumed as a criterion for initiating shear fracture (Chung *et al*, 1977; King *et al*, 1981). In the present case, despite that the shear fracture occurs under the condition of the negative strain rate sensitivity for the majority of specimens, there are still certain specimens with the occurrence under the condition of the positive sensitivity, *e.g.* at temperatures of 233K, 333K and 353K (Fig. 2). Therefore the negative sensitivity requirement does not seem to be a necessity for shear fracture as it is for serrated flow (Penning, 1972; Chung *et al*, 1977; King *et al*, 1981; Huang and Gray, 1990). Regarding the adiabatic effect, an increase in strain rate or a decrease in temperature is generally considered to enhance the susceptibility to the flow localisation and hence, to shear fracture (Rohd, 1973; Chung, *et al*, 1977). However, it is found here that the shear fracture does not occur when temperature is lower than 233K. And, in the temperature range where the shear fracture is evident, the occurrence is dominant at relatively low, rather than high, strain rates. Under the Circumstances, the adiabatic effect is not a direct mechanism inducing the present shear fracture. In view of the present experimental results, it is important to note that the shear fracture and the normal "cup-cone" fracture are both by a process of micro-void coalescence, with the only difference in the dimple shapes on their fracture surfaces. Then the present fracture behaviour is dominated by the macro-mechanism or mode transition instead of the micro-mechanism transition. Consequently the constraint effect is to be evaluated.

The present fractographic observations have provided a direct evidence of the delamination phenomenon which is intensified through the triaxial loading in notch tensile tests (Fig. 2d-f). The phenomenon has also been found in recent years both for conventionally-solidified aluminium alloys (Dorward, 1986; Venkateswara Rao and Ritchie, 1990) and for rapidly-solidified alloys (Porr and Gangloff, 1994). One common characteristics these alloys share is the existence of a certain weak boundary or interface, either the boundary of the mechanically-elongated or flattened grain (Dorward, 1986; Venkateswara Rao and Ritchie, 1990) or the interface of prior powder particle (Porr and Gangloff, 1994). The weak boundary responsible for the present delamination is judged as the interface of prior ribbon flakes which tend to take a longitudinal orientation due to extrusion force. As is shown in Fig. 2-d, local-scale shear fracture occurs in the ligaments between the delaminations. Actually, these ligaments function as individual thin sheets under a loading condition approaching a plane stress state, because the constraint in the neighbourhood is released considerably due to the delaminations. Here there exists a dual-effect resulted from the interaction between the mechanical variant (stress triaxiality introduced by notch) and the metallurgical variant (weak interface). As is commonly the case, triaxiality should promote plane strain fracture (flat fracture). However, when there is a weak interface this same triaxiality can also promote plane stress fracture (shear fracture) due to the delamination of the interface under the action of the transverse stress components, as is the present case. Then the local-scale shear fracture occurring in the notched specimens is promoted by a constraint-releasing mechanism. The delamination also takes place in the smooth tensile specimens of the AE alloy (Fig. 1a-c) although the intensity of the delamination is moderated appreciably compared with the notch tension case. It is important to note that the shear fracture occurs under the condition that the necking process has developed considerably, as is indicated by the magnitude of relative neck curvature a/R. Then it is reasonable to assume the existence of triaxiality (or hydrostatic state) and hence, sizeable transverse stresses. The correction on the hydrostatic stresses results in a radial (or circumferential) stress range of 52 - 64 MPa. Although it is yet difficult to conduct a direct measurement of the interface bonding strength for the present material due to the cylindrical distribution of the prior flakes, the interfacial debonding for some aluminium-based composites has been reported to occur under a

stress level ranging from 10 MPa to 50 MPa (Dhingra and Fishman, 1986; Lin , 1990). This can serve as a reference, indicating that the interfacial bonding strength can be very low and that it is fairly possible for the present delamination to happen under the action of the transverse stress. Anyway, the experimental results declare that the shear fracture in the present condition is always associated with the occurrence of delamination. Therefore the constraint-releasing mechanism is also assumed to account for the shear fracture in smooth tensile bars, as is for the local shearing in notched tensile bars. For the plain tensile case, however, only the central region of the specimen is required to apply this mechanism since the circumferential region is intrinsically in a plane stress state. Assuming this mechanism, the propensity of the alloy to the shear fracture can be clarified regarding its response to temperature and strain rate. According to Eq. 2, the delamination of the weak interface under the action of transverse stresses requires a high flow stress combined with a high value of a/R at the moment of fracture. In the intermediate temperature range, especially at temperatures between 293K and 313K, both flow stress and a/R maintain adequate values to induce a high value of σ_{rr} or $\sigma_{\theta\theta}$. That is why most members of the shear fracture family are located in this intermediate temperature range (Fig. 2). At high temperatures (*e.g.* > 353K), the a/R value is rather high due to an increase in RA, but flow stress at fracture (σ_F) is low. At low temperatures (*e.g.* < 233K), σ_F and a/R exchange their trends. In both cases, the resultant transverse stress level is not sufficient for the occurrence of delamination. Then a restricted regime of temperature and strain rate is justified for locating the shear fracture family (Fig. 2).

SUMMARY

For the recycled Al alloy studied, a complete shear fracture occurs only in the as-extruded plain tensile specimens in a specific range of temperature and strain rate that identifies the shear fracture family. This complete shear fracture has not been observed in the precipitation-hardened group. In the case of notch tension, local shearing is evident between the interfacial delaminations of the prior flakes, suggesting a constraint-releasing mechanism. The shear fracture family is also closely associated with the delamination and the same constraint-releasing mechanism applies. This has been justified further by the prediction of the transverse stress in the necked region, which reasonably accounts for the propensity of delamination in the specified range of temperature and strain rate.

REFERENCES

Asaro, R. J. (1979). Geometrical effects in the inhomogeneous deformation of ductile single crystals, *Acta Metall.*, 27, 445-53.

Backofen, W. A. (1964). *Fracture of Engineering Materials,* ASM, Ohio.

Bridgeman, P. W. (1952). *Studies in Large Plastic Flow and Fracture*, McGraw-Hill, New York.

Chen, C. Q. and H. X. Li (1987). Shear localization in a Al-Zn-Mg-Cu alloy, *Mater. Sci. & Tech.*, 3, 125-30.

Chung, N., J. D. Embury, J. D. Evensen, R. G. Hoagland and C. M. Sargent (1977). Unstable shear failure in a 7075 aluminum alloy, *Acta Metall.*, 25, 377-81.

Dhingra, A. K. and S. G. Fishman (1986). *Interfaces in Metal-Matrix Composites*, The Metallurgical Society, Inc. London.

Dorward, R. C. (1986). Cryogenic toughness of Al-Cu-Li alloy AA 2090, *Scripta Metall.*, 20, 1379-83.

Huang, J. C. and G. T. Gray (1990). Serrated flow and negative sensitivity in Al-Li base alloys, *Scripta Metall. Mater.*, 24, 85-90.

King, J. E., C. P. You and J. F. Knott (1981). Serrated flow and the localized shear failure mode in aluminum alloys, *Acta Metall.*, 29, 1553-66.

Li, D. M. and A. Bakker (1995). Temperature and strain rate dependence of the Portevin - Le Chatelier effect in a rapidly solidified Al alloy, *Metall. Mater. Trans.*, 26A, 2873-79.

Lin, R. Y. (1990). *Interfaces in Metal-Ceramics Composites,* TMS.

Peirce, D., R. J. Asaro and A. Needleman (1982). An analysis of nonuniform and localized deformation in ductile single crystals, *Acta Metall.*, 30, 1087-119.

Penning, P. (1972). Mathematics of the Portevin-Le Chatelier effect, *Acta Metall.*, 20, 1169-75.

Porr, W. C. Jr. and R. P. Gangloff (1994). Elevated temperature fracture of RS/PM alloy 8009: Part I. fracture mechanics behavior, *Metall. Mater. Trans.*, 25A, 365-79.

Rohd, R. W. (1973). *Metallurgical Effects in High Strain Rates,* Plenum Press, New York.

Venkateswara Rao, K. T. and R. O. Ritchie (1990). Mechanism influencing the cryogenic fracture toughness behavior of aluminum-lithium alloys, *Acta Metall. Mater.*, 38, 2309-26.

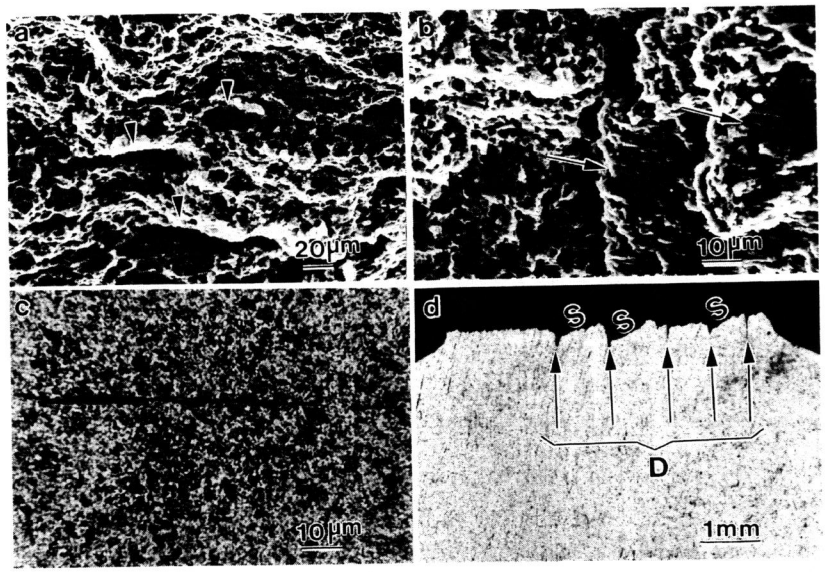

(Fig. 1, to be continued)

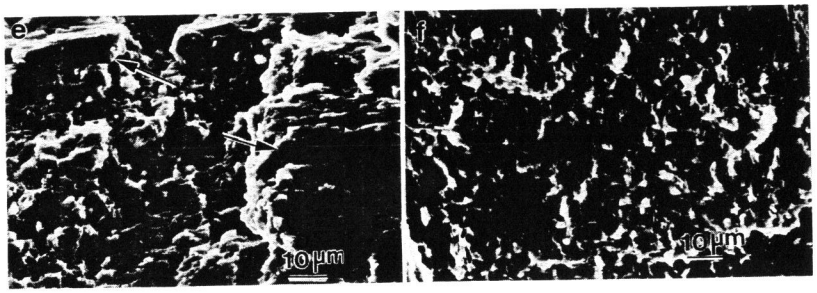

Fig. 1. SEM (*a-b, e-f*) and optical (*c-d*) fractographs for smooth (*a-c*) and notched (*d-f*) tensile specimens of as-extruded alloys: (*a*) secondary cracks formed by interfacial delamination in the central area of fracture surface (no tilt), (*b*) features of the delaminated area (45° tilt), (c) profile showing micro-cracks in the necked region, (*d*) longitudinal profile showing delamination (D) and local shearing (S), (e) details of delaminated interfaces and (f) appearance of local slant fracture surface (~ 45° tilt) as is "S" in (*d*), with tensile axis vertical for (*a*) and (*d*) but horizontal for (*b*), (*c*), (*e*) and (*f*).

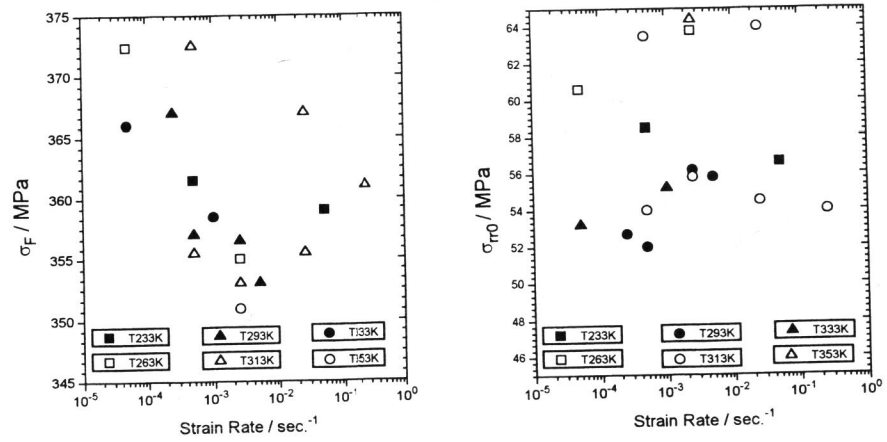

(*a*) (*b*)

Fig. 2. Maps of the shear fracture family: (*a*) corrected fracture stress and (*b*) radial stress at fracture for the cross-sectional centre ($r = 0$).